A hybrid FP-FBG fibre sensor for simultaneous strain and temperature measurement

HE WEI[a,b], ZHAO JIAQI[a], ZHU LIANQING[a,b,*], ZHANG WEN[a,b], DONG MINGLI[a,*], LIU FENG[a]
[a]*Key Laboratory of the Ministry of Education for Optoelectronic Measurement Technology and Instrument, Beijing Information Science & Technology University, Beijing, 100192, China*
[b]*Beijing Laboratory of Optical Fiber Sensing and System, Beijing Information Science & Technology University, Beijing, 100016, China*

A hybrid optical fibre sensor composed of a fibre Bragg grating (FBG) and Fabry-Perot (FP) cavity fabricated by chemical etching was proposed for dual-parameter measurement. The temperature characteristics were measured over the range 30–100 °C. The spectrum of the FP cavity did not shift with temperature, but the sensitivity of the FBG was 9.5 pm/°C (linearity, 0.9994). The sensor showed excellent repeatability. Its strain behaviour was examined in the range 0–550 με. For the FP cavity, the loading and unloading strain sensitivities were 2.8 and 3pm/με, respectively (linearity > 0.9539); for the FBG, these values were both 1.3 pm/με (linearity > 0.9994).

(Received October 19, 2018; accepted October 9, 2019)

Keywords: Fabry-Perot, FBG, Chemical etching, Temperature, Strain, Dual-parameter

1. Introduction

Fibre sensing technology has many advantages, including the capacity for compact structures, high sensitivity, long working life-span, multi-parameter measurement, etc., and therefore it has already been demonstrated for several applications: in the testing of temperature, strain, and refractive index [1-4], and in the fields of structural health monitoring, load testing, spectrum analysis, and biomedicine [5-7]. Methods for single-parameter testing with fiber sensors have been reported [8-9], however, dual-parameter testing is very important in many practical situations, to eliminate cross interference. In order to realize simultaneous dual-parameter measurement, two cascaded sensors, with different sensitivities, are usually adopted. For example, combinations of fibre Bragg grating (FBG), long period grating (LPG), Mach-Zehnder (MZ), Sagnac loop and Fabry-Perot (FP) sensors have been utilised [10-12]. For dual-parameter testing, the sensitivity is determined by testing the performance of each device and from the amount of fusion loss, so two sensors with different sensitivities are usually selected.

Various techniques for fabricating FP-fibre-sensing units have been reported, such as methods based on fibre tapering, fibre tubes, laser machining, and mismatch structures [13-15]. However, in fibre-tube-based FP cavities, the fibre microstructure may be too weak; in fibre-tapering M-Z systems, the fibre sensor is usually too thin; and for laser inscribing, the procedure is extremely complex, and the inscription edge precision is not high; moreover, core diameter mismatch will weaken mechanical strength. Therefore, it is necessary to research an effective method to design a cascaded fibre sensor. Compared with other fibre sensors, an all-fibre FP cavity based on hydrofluoric acid (HF) chemical etching has the beneficial characteristics of high stripe contrast, smooth edges, compact structure, and a simple fabrication process. As one of the most important fibre sensors, the FBG is widely used in temperature and strain measurements because of its high temperature sensitivity, high signal-to-noise ratio (SNR), and narrow linewidth characteristics [16-17]. Consequently, a sensor based on a FP cavity and FBG can be cascaded for dual-parameter testing due to the sensitivities of these sensors.

In the present study, an all-fibre FP cavity was manufactured based on the chemical etching of a single-mode fibre (SMF) to generate an interference spectrum, and a hybrid fibre sensor was fabricated through connecting the FP cavity with a FBG. The proposed fibre sensor can be used for simultaneous dual-parameter measurement. Highly sensitive temperature and strain measurements were simultaneously realized using this sensor, and good temperature stability was achieved.

2. Experiment

The basic structure of the sensor is presented in Fig. 1. The hybrid sensor was composed of a FBG and a FP cavity, and different reflection wavelengths may be obtained simultaneously. In the designed sensor, the FBG was fabricated by ultraviolet exposure using an excimer laser and phase mask; the FP cavity was manufactured by the fibre ending etching method. The single-mode fibre (SMF) core will show faster corrosion speed than the

cladding because the germanium-doped content of fibre core is higher than that of the cladding; HF can therefore be selected to etch grooves at fibre endings. After the corrosion step, the etched fibre was spliced with another SMF of the same size, and the fibre ending surface was cut smoothly. Finally, the air bubble can be created by discharge fusion splicing, as shown in Fig. 2(a,b). For the silica core fibre, the chemical reaction of HF and SiO_2 is expressed in Eq. (1).

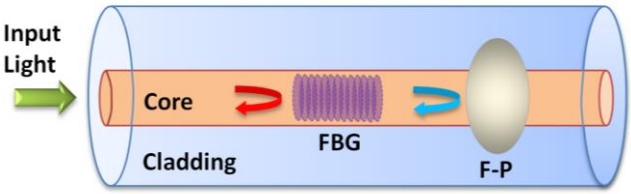

Fig. 1. Schematic diagram of the hybrid fibre sensor

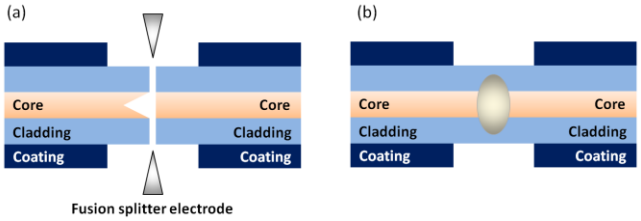

Fig. 2. All-fibre FP air bubble fabrication method. (a) before fusion splicing; (b) after fusion splicing

$$SiO_2 + 6HF \rightarrow 2H_2O + H_2SiF_6 \quad (1)$$

After the FP cavity was manufactured, an interference spectrum was generated, and by connecting it with the FBG, a comb stripe and FBG wavelength can be simultaneously achieved. As shown in Fig. 1, because the size of the FP cavity is larger than the core diameter and thus is in contact with both the fibre core and cladding, the input light will diffuse into the cladding and the transmission will be reduced. In order to improve the spectral performance of the connected FBG and FP cavity, the FBG was designed to be located before FP cavity. For the proposed hybrid sensor, broadband wavelength input light is injected into the SMF, and reflected first by the FBG, and then, the input light is reflected by the FP cavity; therefore, the FP-valley and FBG-peak positions can together be used in the dual-parameter measurement.

When temperature or strain-environment around the hybrid sensor is changed, the size of the FP cavity and FBG period will be influenced, and thus a reflection wavelength shift can be generated. This shift may be expressed as in Eq. (2),

$$\begin{aligned} \Delta\lambda_1 &= K_{11}\Delta T + K_{12}\Delta\varepsilon \\ \Delta\lambda_2 &= K_{21}\Delta T + K_{22}\Delta\varepsilon \end{aligned}, \quad (2)$$

where the wavelength shifts of the FP cavity and the FBG are $\Delta\lambda_1$ and $\Delta\lambda_2$, respectively, and the temperature and strain shifts are ΔT and $\Delta\varepsilon$, respectively. The temperature and strain sensitivity of the FP cavity are respectively K_{11} and K_{12}; and K_{21} and K_{22} are respectively the FBG temperature and strain sensitivity. Thus, the sensing matrix can be constructed using Eq. (3). The invertible matrix is shown in Eq. (4), and the dual-parameter measurement result can be derived after the sensitivity K is determined and the wavelength shift $\Delta\lambda$ is obtained.

$$\begin{bmatrix} \Delta\lambda_1 \\ \Delta\lambda_2 \end{bmatrix} = \begin{bmatrix} K_{11} & K_{12} \\ K_{21} & K_{22} \end{bmatrix} \begin{bmatrix} \Delta T \\ \Delta\varepsilon \end{bmatrix} \quad (3)$$

$$\begin{bmatrix} \Delta T \\ \Delta\varepsilon \end{bmatrix} = \begin{bmatrix} K_{11} & K_{12} \\ K_{21} & K_{22} \end{bmatrix}^{-1} \begin{bmatrix} \Delta\lambda_1 \\ \Delta\lambda_2 \end{bmatrix} \quad (4)$$

3. Results

In the experiment, a SMF-28 fibre (Corning Co.) was used to fabricate the fibre FP cavity; the fibre core/cladding size was 9/125 μm. The FP interferometer spectra and microscope images collected at 5, 10, and 15 min into the etching time are shown in Fig. 3(a–f). After 5 min of etching, the FP spectrum was noisy because of the faulty construction. However, as shown in Fig. 3, the bubble size gradually increased and the wavelength interval progressively decreased as the etching time increased. With very long etching durations, the fibre size will be too thin because of excessive corrosion, and the FP structure too weak; we found that the FP interferometer filter produced by 15 min of etching was sufficiently strong, the bubble diameter size was around 45 μm, and was used in the hybrid sensor. As shown in Fig. 3(f), the fringe spacing, i.e. the distance between two adjacent interference troughs is clear, and this interference wavelength period is 23.3 nm.

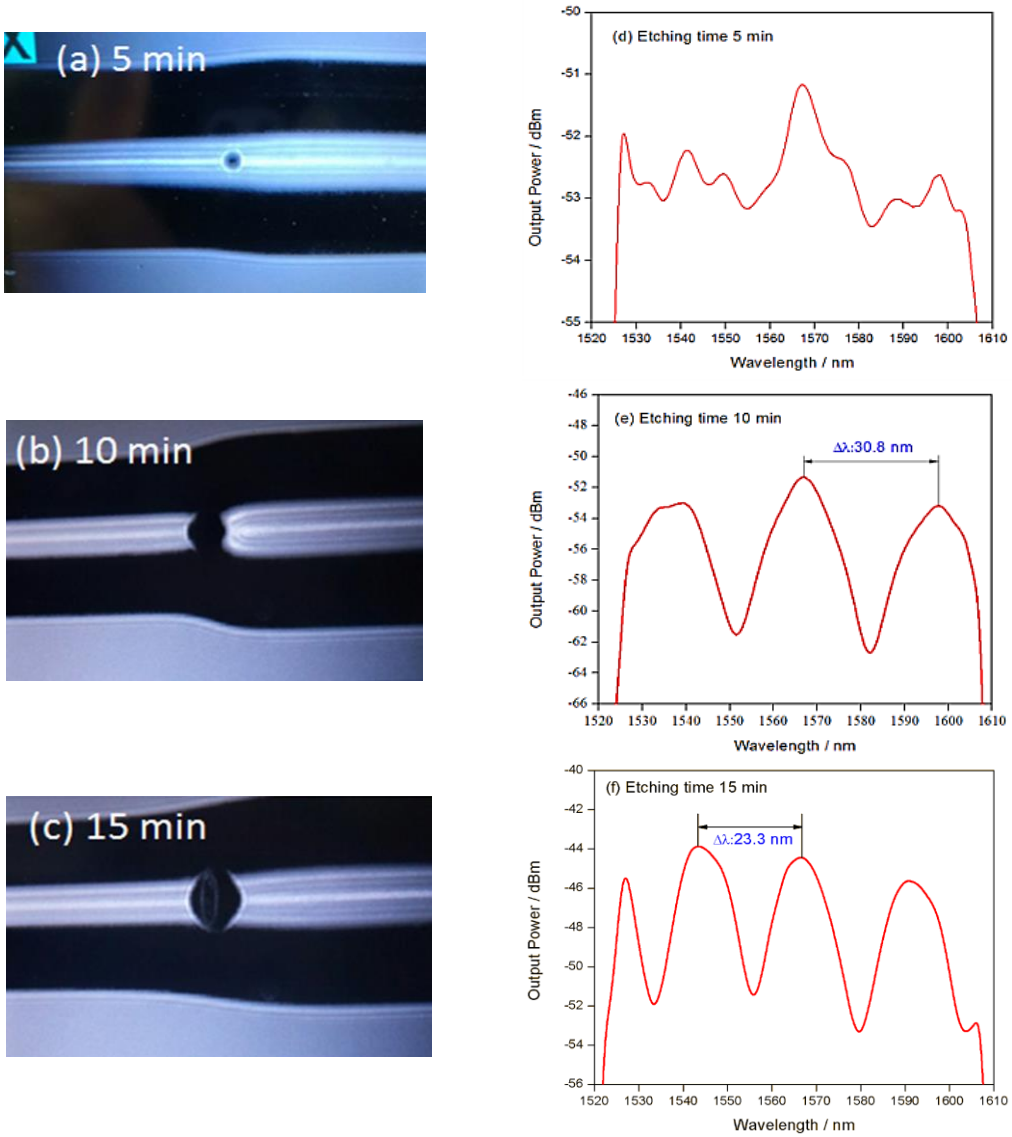

Fig. 3. Microscope images of the FP cavity (left), alongside the FP-cavity spectrum (right) after (a,d) 5, (b,e) 10, and (c,f) 15 min of etching

In the next step, a FBG with a 1563.5-nm reflection wavelength was connected to the FP cavity to form the hybrid sensor. The distance between the two components was 3 cm, and the FBG was fabricated on an SMF-28 fibre using a phase mask and ultraviolet exposure. As shown in Fig. 4, the spectrum performance of the fibre sensor was tested. The testing system was composed of a C+L wavelength band amplified spontaneous emission (ASE) source (1520–1610 nm, Skyrayoe Co.), a circulator (three ports, with FC/APC SMF pigtail fibre, Skyrayoe Co.), and optical spectrum analyser (OSA; Yokogawa Co, AQ6370D). The ASE source was used as the monitoring source. The ASE source and circulator were connected through a fibre connector. The broadband light is injected into the circulator via Port 1, and coupled into the hybrid sensor via Port 2; the reflected light is transmitted from Port 2, through Port 3, to the OSA. An example hybrid-comb spectrum is shown in Fig. 5, where the FP-comb spectrum and the FBG reflection spectrum are obviously distinguishable: the maximum stripe contrast of the FP cavity is 10 dB, and the 3-dB linewidth of the FBG is 0.21 nm.

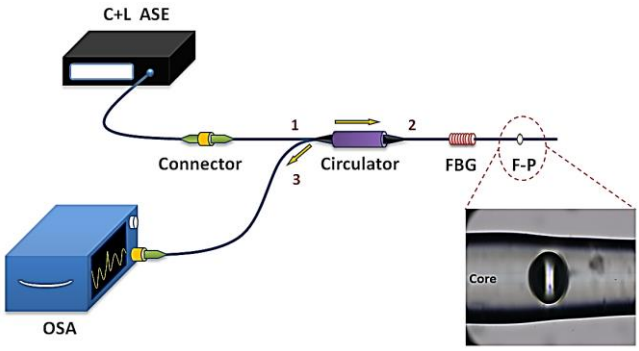

Fig. 4. Schematic diagram of the hybrid sensor testing system

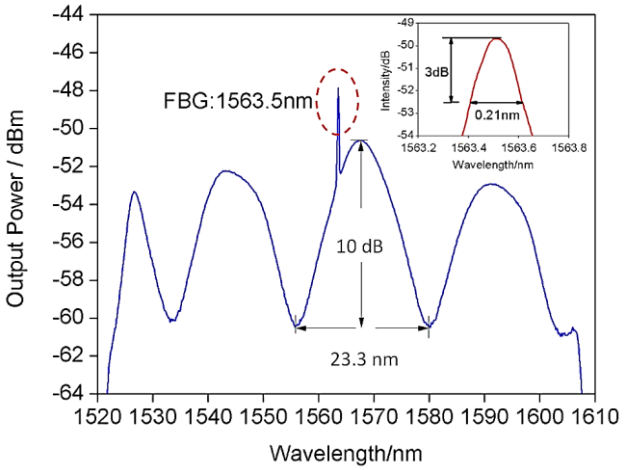

Fig. 5. Hybrid spectrum of the FP cavity and the FBG, with the latter expanded in the inset

The temperature characteristics of the hybrid sensor were tested over the range of 30 to 100 °C using a heating platform, and a reflection spectrum was collected by the OSA at intervals of 10 °C in this range. As shown in Fig. 6(a), the FBG wavelength shifts toward longer wavelengths as the temperature increases. The details of the FBG and FP spectra are shown in Fig. 6(b,c). The linearity of the wavelength shift of the FBG is obvious, and its shifts are much greater than with temperature than are those of the FP cavity. As shown in Fig. 6(d,e), the wavelength shifts and output power fluctuation of the FBG and FP cavity have both been analysed.

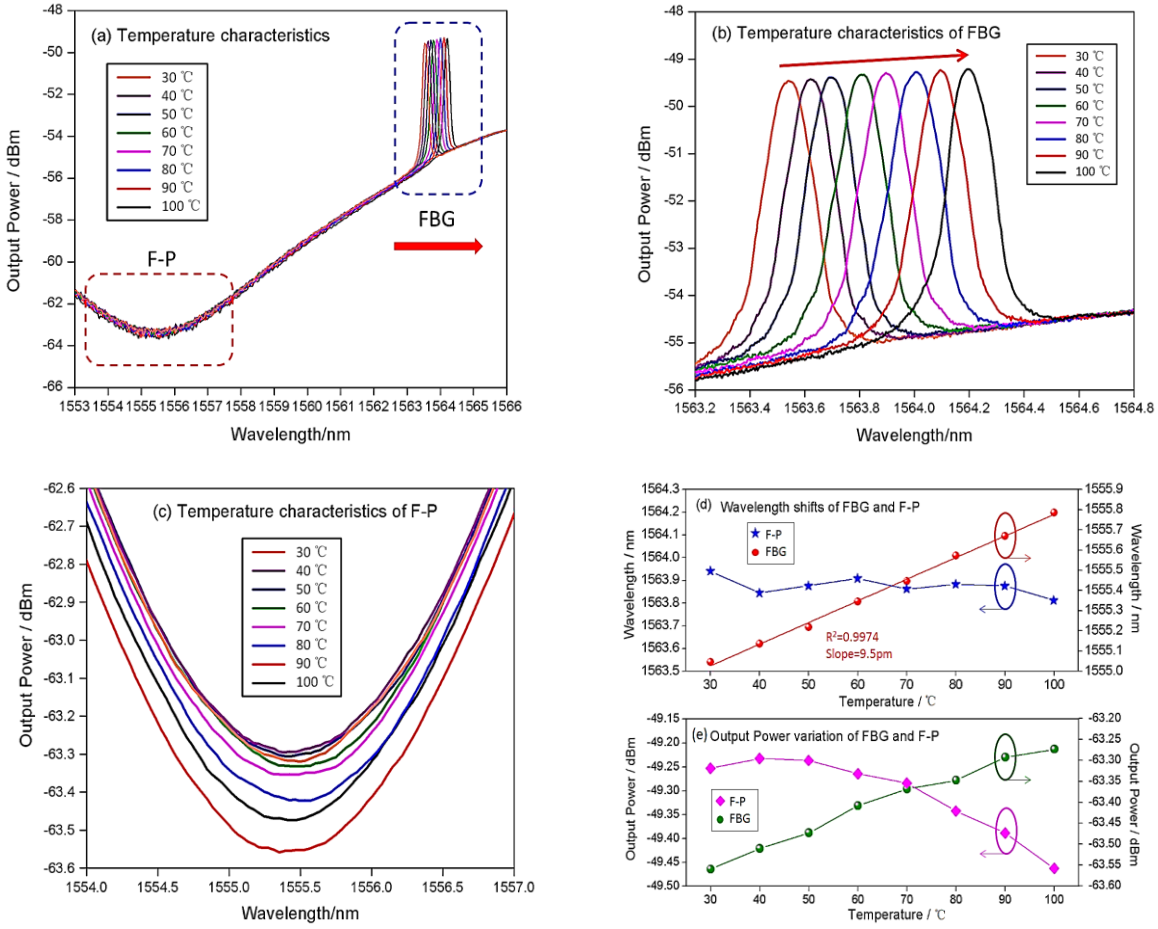

Fig. 6. Temperature dependence of the spectral characteristics of the FBG and FP cavity. (a) spectral variation of the FBG and FP cavity; (b) details of FBG spectral changes; (c) detailed spectral changes of FP cavity; (d) wavelength shifts with temperature; (e) output power variation with temperature

The temperature sensitivity of the FBG wavelength was 9.5 pm/°C, and the linearity was 0.9974, whereas, the FP wavelength was not temperature-sensitive. As temperature increased, the FBG output power was gradually increased, and the variation was 0.27 dB; for the FP cavity, the output power fluctuation was similar (0.26 dB). Thus, for the temperature testing, the FBG showed a higher sensitivity characteristic than the FP cavity. The stability of the hybrid sensor temperature at 100 °C was also measured, as shown in Fig. 7; for 10 min of

monitoring time, wavelength shifts and output power fluctuations were not observed.

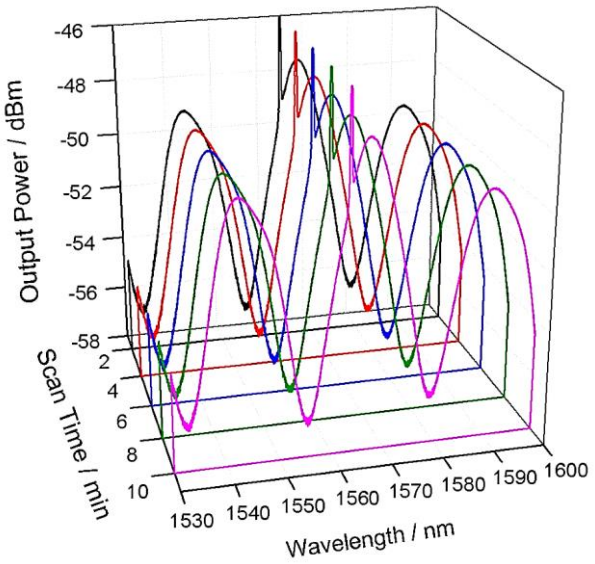

Fig. 7. Temperature stability of hybrid sensor

The strain characteristics of the hybrid sensor were measured between 0 and 550 με, and the reflection spectrum was collected by the OSA at intervals of 50 με. As shown in Fig. 8(a), during the loading phase, both the FBG and FP cavity reflection spectra show obvious movement. The detail spectral variation of the FBG with loading strain is shown in Fig. 8(b), and the wavelength shifts move toward longer wavelengths with increasing strain; for the FP cavity, the wavelength movement also show a red shift (Fig. 8(c)). The linearity of the wavelength shifts of both the FBG and FP cavity with strain are obvious. As shown in Fig. 8(d), the wavelength shifts of the FBG and FP cavity have been analysed; the sensitivity of the FBG wavelength to the loading strain was found to be 1.3 pm/με, and the linearity is 0.9998. The FP-cavity wavelength strain sensitivity and linearity are 2.8 pm/με and 0.9539, respectively. Hence, we conclude that during loading strain phase, the FP cavity has a higher sensitivity characteristic than the FBG.

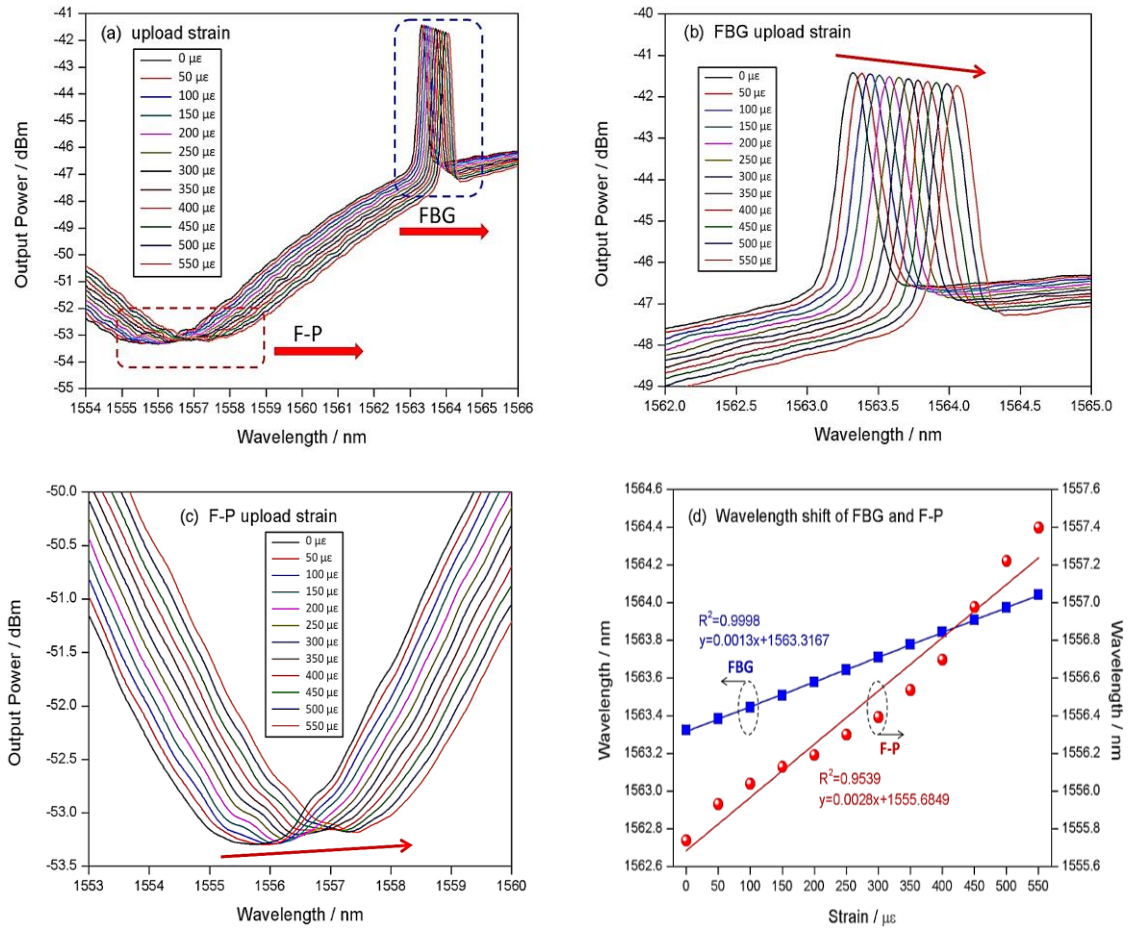

Fig. 8. Spectral characteristics of FBG and FP cavity as a function of loading strain. (a) spectra of FBG and FP cavity; (b) detailed spectral changes of FBG with loading strain; (c) detailed spectral changes of FP cavity with loading strain; (d) wavelength shift as a function of loading strain

The characteristics of the hybrid sensor during the unloading strain phase were also investigated. As shown in Fig. 9(a), for the FBG, the unloading strain sensitivity was 1.3 pm/με and the linearity was 0.9994; whereas, for the FP cavity, the unloading strain sensitivity was 3 pm/με and the linearity was 0.9891 (Fig. 9(b)). During the unloading strain phase, the hybrid sensor displayed excellent consistency, and the FP cavity had an even higher sensitivity characteristic than that of the loading phase.

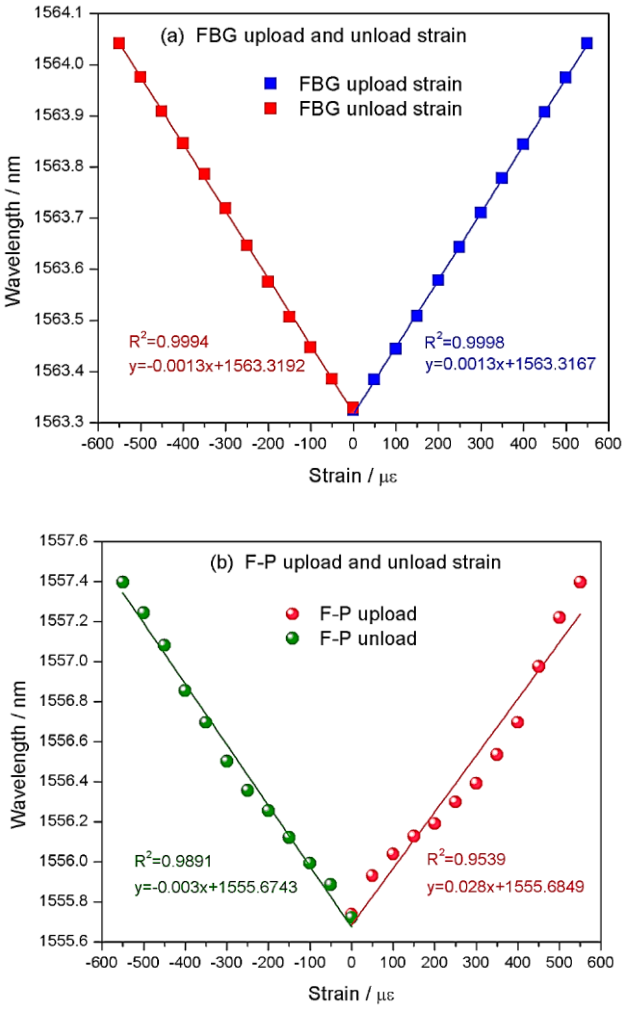

Fig. 9. Wavelength responses to loading and unloading strain in the hybrid sensor

4. Discussion

During the temperature sensitivity measurements, the FBG showed higher sensitivity than the FP cavity, and an obvious wavelength shift of the FP cavity was not observed. The FBG wavelength shifted towards longer wavelengths as temperature increased in the range between 30 and 100 °C. The FBG and FP-cavity temperature sensitivities were found to be 9.5 and 0 pm/°C, respectively. For the strain measurement procedure, the FP cavity was demonstrated to have a higher sensitivity than the FBG, during both loading and unloading strain processes, and the sensitivity values obtained were 2.8 and 1.3 pm/με, respectively. Ultimately, therefore, the dual-parameter matrix can be expressed as follows:

$$\begin{bmatrix} \Delta T \\ \Delta \varepsilon \end{bmatrix} = \begin{bmatrix} 0 & 2.8 \\ 9.5 & 1.3 \end{bmatrix}^{-1} \begin{bmatrix} \Delta\lambda_1 \\ \Delta\lambda_2 \end{bmatrix} \tag{5}$$

5. Conclusions

In this study, an all-fibre hybrid sensor based on a FP cavity and a FBG was proposed and experimentally realized. The fibre FP cavity was manufactured by HF etching, and the wavelength interval was 23.3 nm. Temperature and strain characteristics were measured in the ranges 30–100 °C and 0–550 με, respectively. For the FBG unit, the temperature and strain sensitivities were 9.5 pm/°C and 1.3 pm/με; for the FP-cavity unit, the strain sensitivity was 2.8 pm/με, and it was insensitive to temperature. The proposed fibre sensor was demonstrated to have excellent repeatability and high sensitivity, and can therefore be widely applied in optical sensors, fibre communications, and spectral analysis.

Acknowledgements

This research was Supported by the Programme of Introducing Talents of Discipline to Universities (grant number: D17021); National Natural Science Foundation of China (grant number: 51775051, 61801030); Young Elite Scientists Sponsorship Program by CAST (grant number: 2017QNRC001); and QinXin Talents Cultivation Program Beijing Information Science & Technology University (grant number: QXTCPC201702).

References

[1] H. Ahmad, H. Hassan, A. Z. Zulkifli, K. Thambiratnam, I. S. Amiri, Opt. Quantum Electron. **49**, 207 (2017).
[2] J. Cheng, W. Chen, G. Chen, Opt. Laser Technol. **78B**, 71 (2016).
[3] S. Miclos, D. Savastru, R. Savastru, F. G. Elfarra, I. Lancranjan, Optoelectron Adv. Mat. **13**(1-2), 56 (2019).
[4] H. Haroon, A. Kareem, Optoelectron Adv. Mat. **13**(5-6), 290 (2019).
[5] F. Khan, A. Denasi, D. Barrera, J. Madrigal, S. Sales, S. Misra, IEEE Sens. J. **19**(14), 3211 (2019).
[6] Z. Liu, P. Z. Liu, C. Y. Zhou, Y. C. Huang, L. H.

Zhang, Sensors **19**(13), 2849 (2019).
[7] J. C. Yu, Z. L. Wu, X. Yang, X. Y. Han, M. S. Zhao, Sensors **18**(12), 4478 (2018).
[8] A. Wolf, A. Dostovalov, M. Skvortsov, K. Raspopin, A. Parygin, S. Babin, Opt. Laser Technol. **101**, 202 (2018).
[9] S. Sergiy, E. R. Christian, K. Detlef, Appl. Optics **58**(8), 2076 (2019).
[10] X. Cao, D. Tian, Y. Liu, L. Zhang, T. Wang, IEEE Sens. J. **18**(18), 7481 (2018).
[11] W. Zhang, J. Hao, X. Lou, M. Dong, L. Zhu, Fiber Integr. Opt. **37**(2), 66 (2018).
[12] J. Tan, G. Feng, S. Zhang, J. Liang, W. Li, Y. Luo, Laser Phys. **28**, 075102 (2018).
[13] W. Zhang, J. Hao, M. Dong, X. Lou, L. Zhu, Optik **171**, 632 (2018).
[14] Y. G. Liu, D. Q. Yang, Y. X. Wang, T. Zhang, M. Shao, D. K. Yu, H. W. Fu, Z. A. Jia, Opt. Commun. **443**, 166 (2019).
[15] Y. Liu, X. Liu, H. Fu, Z. Jia, T. Zhang, Opt. Eng. **57**(5), 056104 (2018).
[16] C. Ghosh, V. Priye, Appl. Opt. **57**(24), 6906 (2018).
[17] F. Ren, W. Zhang, Y. Li, Y. Lan, Y. Xie, W. Dai, IEEE Photonics J. **10**(4), 7104309 (2018).

*Corresponding author: zhulianqing@sina.com, dongml@sina.com